International Journal of Engineering Science 192 (2023) 103929

Contents lists available at ScienceDirect

International Journal of Engineering Science

journal homepage: www.elsevier.com/locate/ijengsci

Updated formulation of magnetic body force in ferrofluids

Vinay Kumar [a,b], Van Thanh Dau [a,c], Zia Javanbakht [a], Andrew Seagar [a], Nam-Trung Nguyen [b], Peter Woodfield [a,*]

[a] School of Engineering and Built Environment, Griffith University, Gold Coast, QLD, 4222, Australia
[b] Queensland Micro and Nanotechnology Centre, Brisbane, QLD, 4111, Australia
[c] Centre for Clean Environment and Energy, Griffith University, Gold Coast, QLD, 4222, Australia

A R T I C L E I N F O

Keywords:
Magnetic body force
Ferrofluid
Magnetic field
Thermomagnetic convection
Ferro-hydrodynamics

A B S T R A C T

The magnetic body force is critical for modelling of convection in ferrofluids. Despite a long history in the development of the theories for ferro-hydrodynamics, literature from the last five years shows that a universal consensus has not been reached concerning the formulation of this term for ferrofluids. We present an updated derivation of the body force directly from the Lorentz force and Maxwell's equations. The derivation requires that the differential volume experiencing the body force only contains complete dipole current loops. This has the effect that an additional surface integral term to account for bound surface current is not needed when modelling situations where the ferrofluid has interfaces with other materials. We compare results from our derived body force with five other formulations from the literature for the case of a single conductor in ferrofluid under static and convection conditions. Most formulations become similar in the limit of small magnetic susceptibility. For a susceptibility of the order of 1, as is typical for ferrofluids, the calculated body force from the formulations differed by a factor of about four, greatly affecting thermomagnetic convection predictions for a heated microwire.

1. Introduction

In modelling ferrofluid motion, variations in magnetic fields and magnetic properties due to temperature and concentration gradients induce important body forces. Through such body forces, temperature gradients in ferrofluids subjected to magnetic fields give rise to a unique heat-transfer phenomenon known as 'thermomagnetic convection' that can be used to enhance heat transfer (Priyadharsini & Sivaraj, 2022; Ghosh et al., 2021; Rong et al., 2022). Particle concentration gradients may arise through thermophoresis or magnetophoresis, i.e., the migration of magnetic nanoparticles in the carrier fluid under the influence of temperature gradients and applied magnetic fields, respectively (Khashan et al., 2011a; Khashan et al., 2011b; Leong et al., 2015; Shakiba & Vahedi, 2016; Soltanipour, 2020; Sun et al., 2019). By controlling the parameters of magnetic fields and the properties of ferrofluids, flow patterns can be controlled which opens a variety of applications in cooling enhancement, bio-magnetic separation, drug delivery, and micro-mixing.

Characterising the magnetic body forces allows for the simulation of fluid motion in practical cases. The macroscopic body force in a ferrofluid is the sum of the Lorentz forces at atomic/molecular level, i.e., the forces applied to electrons undergoing partially aligned circular motion in a magnetic field. In continuum fluid dynamics, this force is expressed as a spatial vector field in terms of specific

* Corresponding author.
E-mail address: p.woodfield@griffith.edu.au (P. Woodfield).

https://doi.org/10.1016/j.ijengsci.2023.103929
Received 30 May 2022; Received in revised form 7 July 2023; Accepted 9 July 2023
Available online 23 July 2023
0020-7225/

magnetic field and magnetic material properties. The obtained term is then added to the conventional Navier-Stokes equations as a body force, enabling prediction of the resulting fluid motion through coupling with continuity and energy equations.

Several analytical formulations have been proposed to account for the body force from the principles of ferro-hydrodynamics. However, it is evident from recent discussions (Butcher & Coey, 2023; Cano-Gómez and Romero-Calvo, 2022; Cecchini, & Chiolerio, 2021a; Cecchini, & Chiolerio, 2021b; Engel, 2001; Huang et al., 2019; Liu, 2000; Odenbach & Liu, 2001; Petit et al., 2011; Romero-Calvo et al., 2020) that despite over 50 years since the earliest theoretical studies on ferrofluids (e.g. Neuringer & Rosensweig, 1964**),** a ubiquitous agreement on the form of the magnetic body force has not been reached. Table 1 gives examples of the forms of the body force term used in some recent publications.

Concerning the formulations for the body-force listed in Table 1 and others in the literature, experimental and theoretical work by Odenbach & Liu (2001) and Liu (2000) suggested that $M_i \nabla B_i$ is superior to the Kelvin force, $\mu_0 M_i \nabla H_i$ for ferrofluids. They noted that the two terms become similar in the limit of small susceptibility ($1+\chi \approx 1$) and that for ferrofluids χ is often of the order of 1 or greater (Bakuzis et al. (2005), Vatani et al. (2017)). Fadaei et al. (2017), Hangi et al. (2018), Shaker et al. (2021), and Bahiraei et al. (2019) used the body force $\mu_0 \boldsymbol{M} \cdot \nabla \boldsymbol{H}$ for a static fluid layer. Ashouri and Shafii (2017) and Saedi et al. (2019) used $(\mu_0 \boldsymbol{M} \cdot \nabla)\boldsymbol{H}$ which may be mathematically identical to $\mu_0 \boldsymbol{M} \cdot \nabla \boldsymbol{H}$ depending on the interpretation of $\nabla \boldsymbol{H}$. Romero-Calvo et al. (2020) studied the motion of ferrofluid droplets having susceptibility of 0.181 and found similarity between $\mu_0 \boldsymbol{M} \cdot \nabla \boldsymbol{H}$ and $\boldsymbol{M} \cdot \nabla \boldsymbol{B}$ with additional terms for surface phenomena. Dixit and Pattamatta (2020) made use of result $\mu_0 M \nabla H$ by Rosensweig (1987) where M and H are the magnitudes of $\boldsymbol{M}$ and $\boldsymbol{H}$, respectively. Cecchini and Chiolerio (2021a) and Vatani et al. (2019) used $\nabla(\boldsymbol{M} \cdot \boldsymbol{B})$ for the body force. However, Cano-Gómez and Romero-Calvo (2022) suggested that $\nabla(\boldsymbol{M} \cdot \boldsymbol{B})$ is an inaccurate body force term by showing the disparity between model and experiment results in Romero-Calvo et al. (2020)

Some researchers include surface forces in their analysis. Engel (2001) suggested that a weakness in the study by Odenbach and Liu (2001) was the neglect of surface forces. Romero-Calvo et al. (2020) concluded that inclusion of surface forces is essential when predicting the force on a droplet of ferrofluid. Petit et al. (2011) considered five general expressions for the body force term in ferrofluid including surface forces and concluded that the total force for the bulk material is similar, but the local body force terms are not. These findings have implications for studies in thermomagnetic convection since the local (sub-surface) forces are driving the phenomenon.

The relationship between magnetic susceptibility and temperature is also not in universal agreement. Goharkhah et al. (2020) investigated the three different magnetic force models based on different magnetic susceptibility (χ) correlations as a function of temperature. To investigate the impact on the thermomagnetic convection effects, they compared calculations with experimental results of Vatani et al. (2017) and found significant variations in predicted heat transfer. Their formulations were derived based on $(\boldsymbol{M} \cdot \nabla)\boldsymbol{B}$ where the susceptibility directly influences $\boldsymbol{M}$.

While ferrofluid is treated as a single fluid in many cases, the magnetic body force can be adapted for two-phase numerical analysis including particle-fluid interaction. Apart from estimating drag force, Van der Waals force and surfactant force on ferroparticles, efforts have been made to correctly formulate of the body force model for a complete analysis of magnetophoresis (Sun et al. (2019)). In the studies by Khashan et al. (2011a), Khashan et al. (2011b), Shakiba and Vahedi (2016) and Soltanipour (2020) the term $\mu_0(\boldsymbol{M} \cdot \nabla)\boldsymbol{H}$ is used. As mentioned above, questions have been raised about this form of the body force term for high χ values so further investigation is also valuable for such two-phase applications. Leong et al. (2015) suggested the term $\boldsymbol{M} \cdot \nabla \boldsymbol{B}$ where the volumetric magnetization ($\boldsymbol{M}$) is the function of ferroparticle concentration.

In this study we have compiled and compared commonly used formulations of the body force term in the last two decades. As examples to quantify the significance of differences, we consider a one-dimensional axisymmetric example in a ferrofluid with non-uniform susceptibility and thermomagnetic convection around a heated wire. The motivation for the work is to make further progress towards establishing the most appropriate form of the magnetic body force term for ferrofluid simulation given that there are multiple alternative formulations in current use. The key contribution we aim to make is a presentation of an accessible and systematic derivation of the magnetic body-force term from first principles with parameters clearly defined and assumptions clearly stated.

Table 1
Representative body force terms in recent numerical studies on ferrofluids.

Magnetic body force term	Reference
$(\boldsymbol{M} \cdot \nabla)\boldsymbol{B}$	Goharkhah et al. (2020)
$\mu_0 \boldsymbol{M} \cdot \nabla \boldsymbol{H}$	Hangi et al. (2018), Shaker et al. (2021), Bahiraei et al. (2019), Fadaei et al. (2017)
$\nabla(\boldsymbol{M} \cdot \boldsymbol{B})$	Vatani et al. (2019), Nguyen (2012)
$\mu_0(\boldsymbol{M} \cdot \nabla)\boldsymbol{H}$	Ashouri and Shafii (2017), Saedi et al. (2019), Aminfar et al. (2012, 2013)
$\mu_0 M \nabla H$	Dixit and Pattamatta (2020)

2. Fundamental principles

Understanding the fundamental principles is the key to obtaining the correct formulation of the body force and clarifying any underlying assumptions. Here we state the principles, define the relevant parameters, state assumptions, and derive the expression for the body force term from the Lorentz force.

2.1. Laws of the magnetic field

The body force comes from the motion of electrons in a magnetic field. The magnetic field and its flux density $\boldsymbol{B}$ *can be defined* based on the observed behavior of a moving charge. When a particle of charge q moves with velocity $\boldsymbol{v}$ in a magnetic field of magnetic flux density $\boldsymbol{B}$, then the particle is observed to experience a force $\boldsymbol{F}$ perpendicular to both $\boldsymbol{v}$ and $\boldsymbol{B}$. This force is expressed by the magnetic Lorentz force which we take to be the definition of the $\boldsymbol{B}$-field:

$$\boldsymbol{F} = q\boldsymbol{v} \times \boldsymbol{B}. \tag{1}$$

The vector field $\boldsymbol{B}$ also satisfies the following continuity equation known as Gauss's law for magnetic fields (or Maxwell's second equation)

$$\nabla \cdot \boldsymbol{B} = 0. \tag{2}$$

Eqs. (1) and (2) are true everywhere in the field and require no modification for fields with variations in material properties (such as ferrofluids with temperature gradients or concentration gradients).

The $\boldsymbol{B}$-field arises due to the motion of electric charges and/or changing electric fields. This can be expressed by Ampere's Law (Maxwell's third equation) where the changing electric field has been neglected:

$$\oint_C \boldsymbol{B} \cdot \mathrm{d}\boldsymbol{l} = \mu_0 I_\mathrm{A} = \mu_0 \left(I_{Af} + I_{Ab} \right). \tag{3}$$

In Eq. (3), μ_0 is the permeability of free space and I_A is the total electric current that pierces through the surface A that is bounded by the closed curve, C.

For cases where the line integral C crosses through magnetizable material such as ferrofluid, this equation is still valid but the term on the right-hand side includes contributions from electrons in the material moving in circular paths at a molecular level (bound current, I_Ab). To emphasize this, I_A is divided into bound and free current in Eq. (3).

2.2. Magnetization field M, magnetic field strength H and magnetic properties

Valuable insight into magnetization $\boldsymbol{M}$, magnetic field strength $\boldsymbol{H}$, magnetic susceptibility χ, and magnetic permeability μ, can be gained by considering an infinitely long coil of wire (solenoid) with electrical current I flowing through it as shown in Fig. 1. Here we use this hypothetical experimental setup to unambiguously define the material properties χ and μ for a magnetically 'soft' magnetic material (such as ferrofluid) in a measurable way in terms of the number of turns per unit length of the electrical coil, electrical current, and the magnetic flux density. By 'soft' we mean the fluid does not behave like a permanent magnet, there is no hysteresis in the

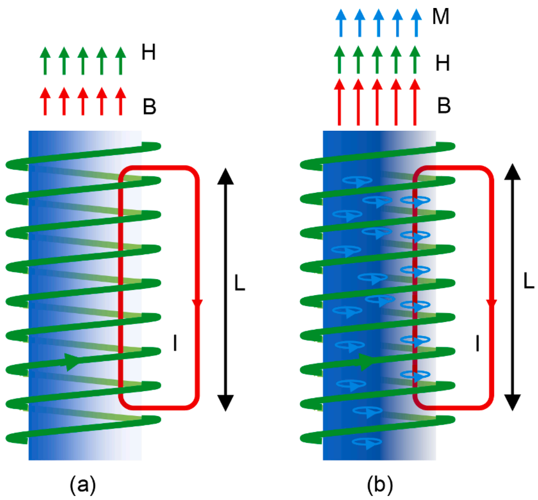

Fig. 1. Physical insight into magnetic field strength and magnetization: H can be considered the number of amp-turns per meter in an infinite solenoid. $\boldsymbol{M}$ can be defined as the effective number of amp-loops per meter in a magnetic material to satisfy Ampere's law. (a) Non-magnetic material, (b) Magnetic material.

magnetization and mechanical equilibrium is quickly reached, (i.e. the relaxation time is small compared with timescales of interest so that ***H, M*** and ***B*** are quickly aligned in situations where the magnetic field changes direction).

Inside the solenoid, magnetic properties and the three vector fields are uniform. *H, M*, and *B* are the magnitudes of ***H, M*** and ***B***, respectively. No additional assumption needs to be made to support the uniformity of the magnetic field inside the coil except that the coil is tightly wound, since the uniformity can be proved easily from Eq. (3). For this case, *H* is the same for both materials (a) and (b) in Fig. 1, while *B* is relatively large for a magnetic material and *M* is zero for the non-magnetic material.

H has units A/m but in terms of Fig. 1, it is insightful to follow an approach used by engineers who design transformers by expressing its units as "amp-turns per meter" (e.g. Chapman (2004). For both Figs. 1a and 1b, from dimensional analysis, "amp-turns per meter" yields:

$H = \frac{NI}{L}$ (applies only to the geometry of Fig. 1).

This is not a general expression for *H* but applies without error or assumption to the configurations of both Fig. 1a and Fig. 1b, where *N* is the number of turns of the solenoid over the axial distance *L*.

The magnetization field is due to microscopic 'bound-current' loops and analogous to *H*, can be considered to be the effective number of amp-loops per meter (drawn as blue circles in Fig. 1b):

$$M = \frac{N_M \langle I_M \rangle}{L},$$

where N_M is the number of atoms encountered along the path *L* inside the material and $\langle I_M \rangle$ is the average bound electrical current that encircles the integration line (following the right-hand rule) per atom, so as to satisfy Ampere's Law. Unlike *H*, scalar components of the magnetization vector ***M*** can *always* be interpreted as the encircling bound current per unit length along a path in the direction of that component through a magnetic material. Thus, generally, the three components of the vector ***M*** can be *defined* by considering paths (that are sufficiently short to be differential but long enough to justify continuum) in the three component directions.

Having defined both ***B*** and ***M*** we are now able to define the magnetic field strength ***H*** (Jackson, (1999)):

$$\boldsymbol{H} \equiv \frac{1}{\mu_0}\boldsymbol{B} - \boldsymbol{M}. \tag{4}$$

This definition of ***H*** is general and applies for cases with strong spatial variations and discontinuities in material properties (where the Biot-Savart law does not apply). In the limit of small property variations in space, the magnetic field strength becomes independent of magnetic properties.

For Fig. 1b, Ampere's law applied to the red loop gives:

$BL = \mu_0 NI + \mu_0 N_M \langle I_M \rangle$.

Comparing this with Eq. (4) shows that *H=NI/L* is appropriate for Fig. 1 and consistent with the definition of ***H***.

In terms of Fig. 1, we can *define* the equilibrium magnetic permeability, μ as:

$$\mu \equiv \frac{B}{H} = \frac{B}{(NI/L)}\Big|_{infinite\ \ solenoid}, \tag{5}$$

where *H* is conveniently determined in terms of measurable geometry and current in the configurations of Fig. 1.

The equilibrium magnetic susceptibility is a dimensionless magnetic material property can be *defined* by comparing the magnetic permeability of a soft magnetic material to that of a vacuum:

$$\chi \equiv \frac{\mu}{\mu_0} - 1. \tag{6}$$

Under the proposed definitions in Eqs. (5) and (6), the permeability and susceptibility are not limited to the linear region of low magnetic field strength but also continue to apply to the saturation region where a larger current is applied to the solenoid in Fig. 1b. Thus, both material properties are generally non-linear functions of the magnetic flux density but may be approximately constant for low magnetic fields. Noting that ***B*** and ***H*** are aligned, the suitable constitutive relationship for ferrofluid consistent with Eqs. (5) and (6) is:

$$\boldsymbol{B} = \mu_0(1+\chi)\boldsymbol{H}. \tag{7}$$

2.3. Treatment of bound current in Ampere's Law

As illustrated in Fig. 1b, the magnetic material may be modelled as many microscopic Amperian dipole loops of electric current, each contributing to the magnetic field in accordance with Ampere's law. The stronger the field ***B***, the better the alignment and the more the magnetic field is enhanced. Here we show that this definition of ***M*** is robust and can be used easily to derive familiar and useful forms of Ampere's Law applicable to ferrofluid.

Since the components of ***M*** may be understood as the encircling bound current per unit length in the component direction, and the Amperian current loops of interest are only those that occur along the path C (e.g. Fig. 1b), Ampere's law (Eq. (3)) becomes:

$$\oint_C \boldsymbol{B} \cdot \mathrm{d}\boldsymbol{l} = \mu_0 I_{Af} + \mu_0 \oint_C \boldsymbol{M} \cdot \mathrm{d}\boldsymbol{l}, \tag{8}$$

where the second term on the right-hand side is the contribution of bound current. Making use of Eqs. (4) and (7), this becomes:

$$\oint_C \boldsymbol{B} \cdot \mathrm{d}\boldsymbol{l} = \mu_0 I_{Af} + \mu_0 \oint_C \frac{\chi}{\mu_0 (1+\chi)} \boldsymbol{B} \cdot \mathrm{d}\boldsymbol{l}.$$

Combining the two integrals gives:

$$\oint_C \boldsymbol{H} \cdot \mathrm{d}\boldsymbol{l} = I_{\mathrm{Af}}.$$

In differential form, this can be written as:

$$\nabla \times \boldsymbol{H} = \boldsymbol{J}_{\mathrm{f}}. \tag{9}$$

where $\boldsymbol{J}_{\mathrm{f}}$ is the electric current density (A/m^2) due to motion of free electrons. Since ferrofluid is typically a poor electrical conductor, Eq. (9) may be simplified to:

$$\nabla \times \boldsymbol{H} = 0. \tag{10}$$

Thus, Ampere's equation in this form is well suited to a ferrofluid with variable magnetic properties and the underlying assumption in Eq. (10) is that the timescale to reach mechanical equilibrium (alignment of ***H*, *M***, and ***B***) is small.

It is useful to also express the differential form of Ampere's law in terms of magnetic flux density. In the limit of a small loop C, the integrals become curls and Eq. (8) becomes:

$$\nabla \times \boldsymbol{B} = \mu_0 \boldsymbol{J}_{\mathrm{f}} + \mu_0 (\nabla \times \boldsymbol{M}) = \mu_0 \boldsymbol{J}_{\mathrm{f}} + \mu_0 \boldsymbol{J}_{\mathrm{b}}. \tag{11}$$

With no free currents this becomes:

$$\nabla \times \boldsymbol{B} = \mu_0 \boldsymbol{J}_{\mathrm{b}}, \tag{12}$$

where $\boldsymbol{J}_{\mathrm{b}}$ is the bound current density. Thus Eq. (12) shows that $\nabla \times \boldsymbol{B} \neq 0$ for ferrofluids since the magnetizable material generally has bound currents. Also, $\nabla \times \boldsymbol{M} \neq 0$ for ferrofluids but rather:

$$\nabla \times \boldsymbol{M} = \boldsymbol{J}_{\mathrm{b}}. \tag{13}$$

Eq. (13) is not an expression of Ampere's law but rather is a mathematical consequence of the cyclic integral on the right-hand side of Eq. (8) becoming a curl in the limit of a vanishingly small integration loop divided by the encircled area.

2.4. Differential magnetic loop model

To obtain the body force, it is necessary to link the Lorentz force (Eq. (1)) to the magnetization and magnetic flux density. Fig. 2 shows our proposed Amperian current loop model to represent the magnetization of a differential element. The differential element is large enough so that there are many microscopic dipole current loops contained within the element (a). The black arrows show the magnetization vector components while the green arrows represent an equivalent flow of electrical current associated this magnetization. The hexahedral shape makes it straight forward to calculate the Lorentz force from the magnetization and the magnetic flux density field, ***B***. It is assumed that the three components can be treated separately, and the principle of superposition applies. Some example Lorentz force components corresponding to the $\hat{\mathbf{e}}_2$ -component of the body force are shown (orange arrows). Similar sets of forces exist for $\hat{\mathbf{e}}_1$ and $\hat{\mathbf{e}}_3$ components. The resultant force divided by the volume of the element gives the required magnetic body force per unit volume on the element.

Each of the forces shown in Fig. 2 can be written down directly from the Lorentz force (Eq. (1)) and the definition of magnetization (encircling bound current per unit length). To do this, Eq. (1) can be re-expressed as:

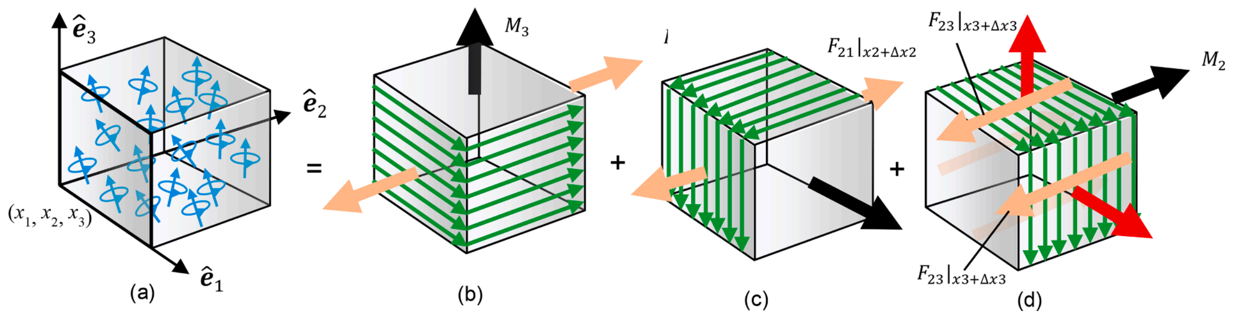

Fig. 2. Differential Amperian Current Loop Model showing contributions to body force in the $\hat{e}_2$ direction (orange arrows). (a) Microscopic current loops, (b) $M_3\Delta x_3$ amps, (c) $M_1\Delta x_1$ amps, (d) $M_2\Delta x_2$ amps

$$\boldsymbol{F} = I\mathrm{d}\boldsymbol{l} \times \boldsymbol{B},$$

where $\boldsymbol{F}$ is the magnetic Lorentz force on a conductor of differential length $\mathrm{d}\boldsymbol{l}$ with electrical current I. For example, for $F_{21}|_{x_2}$ shown in Fig. 2(c), the current is the magnetization component M_1 multiplied by the length of the cell Δx_1, the length of the conductor is the length of the green arrows on the side of the cell (i.e. Δx_3) and the component of $\boldsymbol{B}$ that will cause a Lorentz force in the $\widehat{\mathbf{e}}_2$ direction is $B_1\widehat{\mathbf{e}}_1$. The direction of the green arrows follows the right hand rule for the magnetization. Thus for this force:

$-F_{21}|_{x_2}\widehat{\mathbf{e}}_2 = I\mathrm{d}\boldsymbol{l} \times (B_1\widehat{\mathbf{e}}_1) = (M_1\Delta x_1)(-\Delta x_3\widehat{\mathbf{e}}_3) \times (B_1\widehat{\mathbf{e}}_1) = -(M_1\Delta x_1)\Delta x_3 B_1\widehat{\mathbf{e}}_2.$

It can also be seen in Fig. 2 that the forces come in pairs. For example, using the first term of the Taylor series expansion for B_1 at position $x_2+\Delta x_2$:

$-F_{21}|_{x2} + F_{21}|_{x2+\Delta x2} = -(M_1\Delta x_1)\Delta x_3 B_1 + (M_1\Delta x_1)\Delta x_3\left(B_1 + \Delta x_2\frac{\partial B_1}{\partial x_2} + \cdots\right) = M_1\Delta x_1\Delta x_2\Delta x_3\frac{\partial B_1}{\partial x_2}.$

Adding all the forces for the $\widehat{\mathbf{e}}_2$ direction and dividing by the volume of the element gives:

$f_2 = M_1\frac{\partial B_1}{\partial x_2} + M_3\frac{\partial B_3}{\partial x_2} - M_2\frac{\partial B_1}{\partial x_1} - M_2\frac{\partial B_3}{\partial x_3}.$

Making use of Maxwell's 2nd Law (Eq. (2)) gives

$f_2 = M_1\frac{\partial B_1}{\partial x_2} + M_2\frac{\partial B_2}{\partial x_2} + M_3\frac{\partial B_3}{\partial x_2}.$

Similarly

$$f_1 = M_1\frac{\partial B_1}{\partial x_1} + M_2\frac{\partial B_2}{\partial x_1} + M_3\frac{\partial B_3}{\partial x_1},$$

and

$f_3 = M_1\frac{\partial B_1}{\partial x_3} + M_2\frac{\partial B_2}{\partial x_3} + M_3\frac{\partial B_3}{\partial x_3}.$

This gives our derived form of the magnetic body force in Cartesian coordinates. Note that the same result will appear if magnetization is defined as the "magnetic moment density" (Jackson, 1999). For the model in Fig. 2, there is only one magnetic moment for each component direction, where the magnetic moment is given by the encircling current multiplied by the area encircled. For example, for the $\widehat{\mathbf{e}}_3$ direction, the magnetic moment is the bound current shown by green arrows in Fig. 2b multiplied by $\Delta x_1\Delta x_2$. To obtain the magnetic moment density, this is divided by the volume of the element, giving M_3 as the encircling current divided by Δx_3 (i.e. encircling bound current per unit length). In Einstein tensor form the derived body force can be expressed as:

$$f_j = M_i\frac{\partial B_i}{\partial x_j}. \tag{14}$$

Alternatively, it can be expressed in regular tensor notation as:

$$\boldsymbol{f}_b = (\nabla\boldsymbol{B})\cdot\boldsymbol{M}. \tag{15}$$

While Eq. (14) is very clear in its interpretation, Eq. (15) could be ambiguous. The convention we use for $(\nabla\boldsymbol{B})$ follows the dyadic product and can be found in Kuo and Acharya (2012), Papanastasiou et al. (2021) and Brand (2020). Kuo and Acharya (2012) give expressions for this tensor in other coordinate systems. In Cartesian coordinates, it is given by:

$$\nabla\boldsymbol{B} \equiv \begin{bmatrix} \frac{\partial B_1}{\partial x_1} & \frac{\partial B_2}{\partial x_1} & \frac{\partial B_3}{\partial x_1} \\ \frac{\partial B_1}{\partial x_2} & \frac{\partial B_2}{\partial x_2} & \frac{\partial B_3}{\partial x_2} \\ \frac{\partial B_1}{\partial x_3} & \frac{\partial B_2}{\partial x_3} & \frac{\partial B_3}{\partial x_3} \end{bmatrix}$$

It might be desirable to express Eq. (15), in a different form using the vector calculus identity:

$(\nabla\boldsymbol{B})\cdot\boldsymbol{M} = (\boldsymbol{M}\times\nabla)\times\boldsymbol{B} + \boldsymbol{M}(\nabla\cdot\boldsymbol{B}).$

Noting Eq. (2), the recommended body force term can be re-expressed as:

$$\boldsymbol{f}_b = (\boldsymbol{M}\times\nabla)\times\boldsymbol{B}. \tag{16}$$

A further vector calculus identity gives another equivalent expression:

$$\boldsymbol{f}_b = (\nabla\boldsymbol{B})\cdot\boldsymbol{M} = (\boldsymbol{M}\cdot\nabla)\boldsymbol{B} + \boldsymbol{M}\times(\nabla\times\boldsymbol{B}). \tag{17}$$

3. Alternative derivation from integral forms of Lorentz force

In several studies related to the body force, the analysis is divided into two components — a body force on the inside of the material and a surface force on the outside. This raises a question as to whether our derived body force (Eq. (15)) could also be found from the integral forms of the Lorentz force. Here we show that the same result is obtained.

The total Lorentz force for a volume V with external surface A is given by:

$$\boldsymbol{F} = \int_V \boldsymbol{J}_b \times \boldsymbol{B}\, \mathrm{d}V + \int_A \boldsymbol{K}_b \times \boldsymbol{B}\, \mathrm{d}A. \tag{18}$$

where $\boldsymbol{J}_\mathrm{b}$ is the bound current density (A/m^2) inside the material and $\boldsymbol{K}_\mathrm{b}$ is the bound current per unit length (A/m) on the surface of the material. The 2$^{\mathrm{nd}}$ term on the right-hand side of Eq. (18) is necessary if the surface current is not captured by $\boldsymbol{J}_\mathrm{b}$. Note that we have already found an expression for $\boldsymbol{J}_\mathrm{b}$ in Eq. (13). Fig. 3 shows why Eq. (13) does not capture the surface bound current. The curl in Eq. (13) is the result of taking the limit of an infinitesimally small path of integration for $\oint_C \boldsymbol{M} \cdot \mathrm{d}\boldsymbol{l}$. In the case of an internal path, the current enclosed by the red integration path in Fig. 3 includes the currents of two neighboring dipoles which tend to almost cancel each other. This cancelling effect does not happen on the surface and thus the bound surface current per unit length must be summed up only on the boundary; namely, an outward normal director to the surface $\widehat{\mathbf{n}}$ can be used to collect the boundary current:

$$\boldsymbol{K}_b = \boldsymbol{M} \times \widehat{\mathbf{n}}. \tag{19}$$

A general expression derived from Eq. (13) that could account for any step change in magnetization is:

$$\boldsymbol{K}_b = \widehat{\mathbf{n}} \times (\boldsymbol{M}_{outside} - \boldsymbol{M}_{inside}). \tag{20}$$

where $\boldsymbol{M}_{\mathrm{outside}}$ is the magnetization of the neighboring material outside the boundary and $\boldsymbol{M}_{\mathrm{inside}}$ is magnetization of the material inside the boundary. If $\boldsymbol{M}_{\mathrm{outside}}$ is zero, Eq. (20) reduces to Eq. (19).

In most discussions in the literature, the 2$^{\mathrm{nd}}$ term on the right of Eq. (18) is applied to the external surface of the magnetic material where the interface is with a non-magnetic material (such as air at the boundary of the magnetic fluid). However, Fig. 4 shows that both integrals are also necessary to find the body force on an *internal* volume surrounded by the same type of magnetic material (i.e. ferrofluid) if dipole current loops are treated as being indivisible (i.e. the internal volume only contains complete bound current loops). In the case of ferrofluid, the Lorentz force is applied to moving electrons in the magnetic particles which pass the force to the solid and then to the fluid. Therefore, when considering the body force exerted on the fluid, the boundary of the internal volume should only contain complete nanoparticles and therefore complete dipole current loops (as illustrated in Fig. 4). Hence, for a differential volume completely surrounded by ferrofluid, there is an internal interface where the carrier fluid with a magnetization of zero is adjacent to the solid magnetic material and Eq. (19) applies.

Substituting Eq. (13) and Eq. (19) into Eq. (18) gives:

$$\boldsymbol{F} = \int_V (\nabla \times \boldsymbol{M}) \times \boldsymbol{B}\, \mathrm{d}V + \int_A (\boldsymbol{M} \times \widehat{\boldsymbol{n}}) \times \boldsymbol{B}\, \mathrm{d}A. \tag{21}$$

By applying the Gauss-Ostrogradsky theorem (Eremeyev et al. (2018)), the surface and volume integrals can be related together for the second term on the right-hand side of Eq. (21) (see Appendix):

$$\int_A (\mathbf{M} \times \widehat{\mathbf{n}}) \times \mathbf{B}\, \mathrm{d}\mathbf{A} = \int_{\mathbf{V}} [(\nabla \mathbf{M}) \cdot \mathbf{B} + (\nabla \mathbf{B}) \cdot \mathbf{M} - (\nabla \cdot \mathbf{B})\mathbf{M} - \mathbf{B} \cdot (\nabla \mathbf{M})]\mathrm{d}\mathbf{V}. \tag{22}$$

The first term on the right-hand side of Eq. (21) can be rearranged (see Appendix) to give:

$$\int_V (\nabla \times \boldsymbol{M}) \times \boldsymbol{B}\, \mathrm{d}V = \int_V -(\nabla \boldsymbol{M}) \cdot \boldsymbol{B} + \boldsymbol{B} \cdot (\nabla \boldsymbol{M})\, \mathrm{d}V. \tag{23}$$

Substituting Eq. (22) and Eq. (23) into Eq. (21) gives

$$\boldsymbol{F} = \int_V [-(\nabla \cdot \boldsymbol{B})\boldsymbol{M} + (\nabla \boldsymbol{B}) \cdot \boldsymbol{M}]\, \mathrm{d}V.$$

Making use of Maxwell's 2$^{\mathrm{nd}}$ Law (Eq. (2)) gives

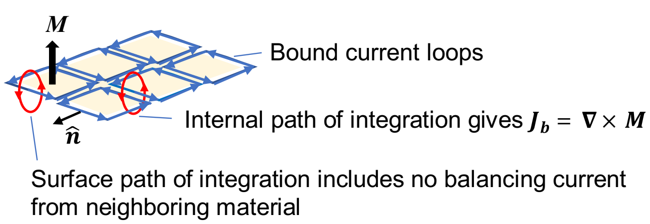

Fig. 3. Distinction between surface and internal bound currents

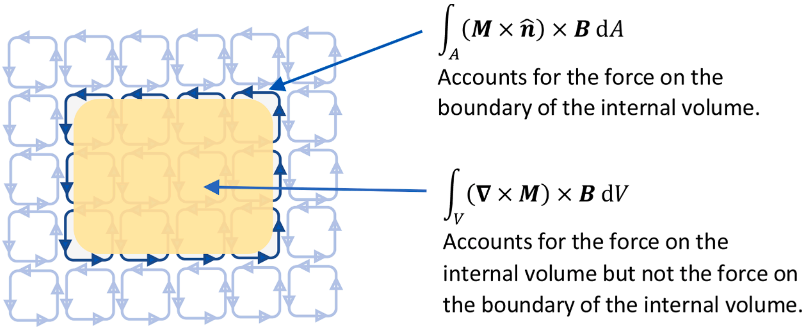

Fig. 4. Illustration of the Lorentz force integrals on an internal volume representing Amperian bound current loops with arrows in the direction of the current flow

$$\boldsymbol{F} = \int_V (\nabla \boldsymbol{B}) \cdot \boldsymbol{M}\, \mathrm{d}V. \tag{24}$$

Thus, per unit volume, the body force is that given previously in Eq. (15). Moreover, this analysis shows that if this body force form (Eq. (15)) is used, it is unnecessary to add another magnetic force to the outside surface (even for free-surface studies) since the surface force is already included in the body force.

4. Relation to force on a single magnetic dipole moment

From classical electrodynamics (Jackson 1999), the force on a single magnetic dipole moment $\boldsymbol{m}$ is given by:

$$\boldsymbol{F}_{dp} = \nabla(\boldsymbol{m} \cdot \boldsymbol{B}). \tag{25}$$

Since magnetization $\boldsymbol{M}$ can be defined as the magnetic moment density we have:

$$\boldsymbol{M} = \frac{1}{\Delta V} \sum \boldsymbol{m}, \tag{26}$$

where ΔV is the volume of a differential element and the summation includes to all magnetic dipoles within the element. The magnetic body force term is the summation of the force on all dipoles within the element divided by the volume. From Eq. (25) this can be given by:

$$\boldsymbol{f}_b = \frac{1}{\Delta V} \sum \nabla(\boldsymbol{m} \cdot \boldsymbol{B}). \tag{27}$$

Is it valid to swap the order of summation and differentiation and substitute Eq. (26) into Eq. (27) to arrive at $\nabla(\boldsymbol{M} \cdot \boldsymbol{B})$for the magnetic body force? There is a problem in that $\boldsymbol{M}$ and $\boldsymbol{m}$ have a distinctly different property that becomes apparent when the differential operator ∇ is applied – that is, the magnetic moment of a single dipole $\boldsymbol{m}$ is a constant with respect to space, while the magnetization $\boldsymbol{M}$ is spatially variant. So if Eq. (27) is expanded out into components, all derivatives of the components of $\boldsymbol{m}$ will vanish. On the other hand, if the order of summation and differentiation is swapped and Eq. (26) is substituted into Eq. (27), the spatial derivatives of $\boldsymbol{M}$ will remain, giving a different body force.

This problem can be avoided by applying the following tensor identity to Eq. (25):

$$\boldsymbol{F}_{dp} = \nabla(\boldsymbol{m} \cdot \boldsymbol{B}) = (\nabla \boldsymbol{B}) \cdot \boldsymbol{m} + (\nabla \boldsymbol{m}) \cdot \boldsymbol{B} \tag{28}$$

Since the single dipole moment $\boldsymbol{m}$ is spatially invariant, $\nabla \boldsymbol{m}$ is zero and the force on the single dipole is given by:

$$\boldsymbol{F}_{dp} = (\nabla \boldsymbol{B}) \cdot \boldsymbol{m} \tag{29}$$

Again applying the summation of all forces on individual magnetic dipoles within the differential volume and dividing by ΔV:

$$\boldsymbol{f}_b = \frac{1}{\Delta V} \sum ((\nabla \boldsymbol{B}) \cdot \boldsymbol{m}) = (\nabla \boldsymbol{B}) \cdot \left(\frac{1}{\Delta V} \sum \boldsymbol{m} \right) \tag{30}$$

For Eq. (30), we can substitute the magnetization from Eq. (26) without the concern that individual dipoles are constants while the magnetic dipole density $\boldsymbol{M}$ is spatially variant, since no spatial derivatives are applied to the summation. This reasoning gives (in agreement with Eq. (15):

$$\boldsymbol{f}_b = (\nabla \boldsymbol{B}) \cdot \boldsymbol{M}$$

5. Practical comparisons of formulations

While the above derivations are strongly in favor of $(\nabla \boldsymbol{B}) \cdot \boldsymbol{M}$ as the appropriate formulation for the body force term, it is yet unclear how different the most commonly used forms shown in Table 1 are from each other. To illustrate this, we consider two examples. The first is shown in Fig. 5 and has an exact analytical solution. The second makes use of computational fluid dynamics simulation to find the effect of the different body force formulations on thermomagnetic convection.

5.1. Analytical test case

Fig. 5 represents an infinitely long circular conductor immersed in a magnetic fluid. The dimensions and values have been selected to approximately correspond to our previous experimental work (Kumar et al., 2021). To simplify the problem, it is assumed that there is no thermomagnetic convection, and the domain is axisymmetric. The magnetic susceptibility varies linearly in the radial direction. r_w is the radius of the wire and R is the radius of the domain to be plotted.

Applying Ampere's law to the configuration gives the following solution for the magnetic flux density:

$$B_\theta = \frac{\mu_0 (1+\chi) I}{2\pi r}, \tag{31}$$

where B_θ is the azimuthal component of the magnetic flux density. Axial and radial components of $\boldsymbol{B}$ for this axisymmetric case (where χ varies only in the radial direction) are zero.

Table 2 provides a summary of six different formulations from the literature including equivalent tensor notations and the full expression of the vector components in Cartesian coordinates. The final column on the right gives the form of the term relevant to the 1D axisymmetric example case in Fig. 5. The detailed forms were derived by expressing the magnetic flux density (Eq. (31)), the magnetic field strength and magnetization and their derivatives in Cartesian coordinates. For example:

$$B_1 = \frac{-\mu_0 (1+\chi) I x_2}{2\pi (x_1^2 + x_2^2)},$$

$$B_2 = \frac{\mu_0 (1+\chi) I x_1}{2\pi (x_1^2 + x_2^2)},$$

$$\frac{\partial B_1}{\partial x_1} = \frac{\mu_0 I x_2}{2\pi (x_1^2 + x_2^2)} \left(-\frac{\partial \chi}{\partial x_1} + \frac{2x_1 (1+\chi)}{(x_1^2 + x_2^2)} \right),$$

$$\frac{\partial B_1}{\partial x_2} = \frac{\mu_0 I}{2\pi (x_1^2 + x_2^2)} \left(-1 - \chi - x_2 \frac{\partial \chi}{\partial x_2} + \frac{2x_2^2 (1+\chi)}{(x_1^2 + x_2^2)} \right).$$

Expressions like these can easily be differentiated to assemble all the terms in the various formula for the magnetic body force in Table 2 for calculating the body force.

It may be observed from right-most column of Table 2 that in the limits of small susceptibility (compared with unity) and small spatial gradients in susceptibility that all formulations approach the same result $(-\chi \mu_0 I^2 / (4\pi^2 r^3))$ except $\nabla(\boldsymbol{M} \cdot \boldsymbol{B})$ (case (c)) which approaches $(-\chi \mu_0 I^2 / (2\pi^2 r^3))$. Thus, for this limit case (c) is double in magnitude. For the example of an infinite wire in ferrofluid, cases (d), (e) and (f) all give the same result which differs in magnitude from cases (a) and (b) by the factor $(1+\chi)$ if spatial gradients in susceptibility are small.

The vector identity:

$$(\nabla \boldsymbol{B}) \cdot \boldsymbol{M} = (\boldsymbol{M} \cdot \nabla) \boldsymbol{B} + \boldsymbol{M} \times (\nabla \times \boldsymbol{B}),$$

shows that cases (a) and (b) differ from each other by $\boldsymbol{M} \times (\nabla \times \boldsymbol{B})$. Sometimes in the literature it is noted that $(\nabla \times \boldsymbol{B})$ is approximately zero based on Ampere's law if bound currents are small (see Eq. (12)). In a similar way it can be shown that cases (d) and (f) are identical if use is made of Eq. (10) $(\nabla \times \boldsymbol{H} = 0)$. It may be noticed in Table 2 that cases (b) and (c) include terms involving $\partial \chi / \partial r$ while case (a) does not. This is because, for this particular problem, $(\boldsymbol{M} \cdot \nabla)\boldsymbol{B}$ simplifies to $f_r = -M_\theta B_\theta / r$.

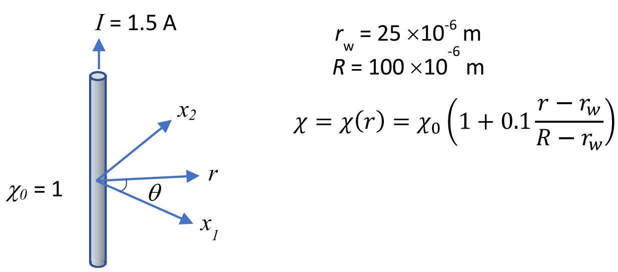

Fig. 5. Test case with radially varying susceptibility

Table 2
Various formulations for the magnetic body force density in ferrofluid.

S. No.	Tensor notations	Cartesian coordinates	Ref.	Magnitude of force density for test case	$f_{b,max}$ $\left(\frac{N}{m^3}\right)$
(a)	$(\boldsymbol{M}\cdot\nabla)\boldsymbol{B}$	$\begin{bmatrix} M_1\frac{\partial B_1}{\partial x_1}+M_2\frac{\partial B_1}{\partial x_2}+M_3\frac{\partial B_1}{\partial x_3} \\ M_1\frac{\partial B_2}{\partial x_1}+M_2\frac{\partial B_2}{\partial x_2}+M_3\frac{\partial B_2}{\partial x_3} \\ M_1\frac{\partial B_3}{\partial x_1}+M_2\frac{\partial B_3}{\partial x_2}+M_3\frac{\partial B_3}{\partial x_3} \end{bmatrix}$	Mukhopadhyay et al. (2005), Ganguly et al. (2004)	$\frac{-\chi(1+\chi)\mu_0 I^2}{4\pi^2 r^3}$	7.64×10^6
(b)	$(\nabla\boldsymbol{B})\cdot\boldsymbol{M}$ $M_i\left(\frac{\partial B_i}{\partial x_j}\right)$	$\begin{bmatrix} M_1\frac{\partial B_1}{\partial x_1}+M_2\frac{\partial B_2}{\partial x_1}+M_3\frac{\partial B_3}{\partial x_1} \\ M_1\frac{\partial B_1}{\partial x_2}+M_2\frac{\partial B_2}{\partial x_2}+M_3\frac{\partial B_3}{\partial x_2} \\ M_1\frac{\partial B_1}{\partial x_3}+M_2\frac{\partial B_2}{\partial x_3}+M_3\frac{\partial B_3}{\partial x_3} \end{bmatrix}$	Odenbach and Liu (2001), Liu (2000)	$\frac{-\chi(1+\chi)\mu_0 I^2}{4\pi^2 r^3}\left(1-\frac{r}{1+\chi}\frac{\partial\chi}{\partial r}\right)$	7.49×10^6
(c)	$\nabla(\boldsymbol{M}\cdot\boldsymbol{B})$ $\frac{\partial(M_iB_i)}{\partial x_j}$	$\begin{bmatrix} \frac{\partial M_1B_1}{\partial x_1}+\frac{\partial M_2B_2}{\partial x_1}+\frac{\partial M_3B_3}{\partial x_1} \\ \frac{\partial M_1B_1}{\partial x_2}+\frac{\partial M_2B_2}{\partial x_2}+\frac{\partial M_3B_3}{\partial x_2} \\ \frac{\partial M_1B_1}{\partial x_3}+\frac{\partial M_2B_2}{\partial x_3}+\frac{\partial M_3B_3}{\partial x_3} \end{bmatrix}$	Nguyen (2012), Vatani et al. (2019)	$\frac{-\chi(1+\chi)\mu_0 I^2}{4\pi^2 r^3}\left(2-\frac{r(1+2\chi)}{\chi(1+\chi)}\frac{\partial\chi}{\partial r}\right)$	14.9×10^6
(d)	$\mu_0(\nabla\boldsymbol{H})\cdot\boldsymbol{M}$ $\mu_0 M_i\left(\frac{\partial H_i}{\partial x_j}\right)$	$\mu_0\begin{bmatrix} M_1\frac{\partial H_1}{\partial x_1}+M_2\frac{\partial H_2}{\partial x_1}+M_3\frac{\partial H_3}{\partial x_1} \\ M_1\frac{\partial H_1}{\partial x_2}+M_2\frac{\partial H_2}{\partial x_2}+M_3\frac{\partial H_3}{\partial x_2} \\ M_1\frac{\partial H_1}{\partial x_3}+M_2\frac{\partial H_2}{\partial x_3}+M_3\frac{\partial H_3}{\partial x_3} \end{bmatrix}$	-	$\frac{-\chi\mu_0 I^2}{4\pi^2 r^3}$	3.06×10^6
(e)	$\mu_0 M\nabla H$ $\mu_0 M\left(\frac{\partial H}{\partial x_j}\right)$	$\mu_0 M\begin{bmatrix} \frac{\partial}{\partial x_1}\sqrt{H_1^2+H_2^2+H_3^2} \\ \frac{\partial}{\partial x_2}\sqrt{H_1^2+H_2^2+H_3^2} \\ \frac{\partial}{\partial x_3}\sqrt{H_1^2+H_2^2+H_3^2} \end{bmatrix}$	Dixit and Pattamatta (2020), Rosensweig (1987), Rahman and Suslov (2015)	$\frac{-\chi\mu_0 I^2}{4\pi^2 r^3}$	3.06×10^6
(f)	$\mu_0(\boldsymbol{M}\cdot\nabla)\boldsymbol{H}$ $\mu_0 M_i\left(\frac{\partial H_j}{\partial x_i}\right)$	$\mu_0\begin{bmatrix} M_1\frac{\partial H_1}{\partial x_1}+M_2\frac{\partial H_1}{\partial x_2}+M_3\frac{\partial H_1}{\partial x_3} \\ M_1\frac{\partial H_2}{\partial x_1}+M_2\frac{\partial H_2}{\partial x_2}+M_3\frac{\partial H_2}{\partial x_3} \\ M_1\frac{\partial H_3}{\partial x_1}+M_2\frac{\partial H_3}{\partial x_2}+M_3\frac{\partial H_3}{\partial x_3} \end{bmatrix}$	Ashouri and Shafii, (2017), Saedi et al. (2019)	$\frac{-\chi\mu_0 I^2}{4\pi^2 r^3}$	3.06×10^6

In Fig. 6, the Cartesian coordinate formulation in Table 2 has been applied to the case shown in Fig. 5. To make the example axisymmetric, we assumed that the susceptibility does not vary in the azimuthal direction. For simplicity, it is assumed to vary linearly in the radial direction with a 10% variation across the domain under investigation as:

$$\chi=\chi_0\left(1+0.1\frac{\sqrt{x_1^2+x_2^2}-r_w}{R-r_w}\right).$$

Gradients in susceptibility are thus

$$\frac{\partial\chi}{\partial x_1}=\chi_0\frac{0.1x_1}{(R-r_w)\sqrt{x_1^2+x_2^2}},$$

$$\frac{\partial\chi}{\partial x_2}=\chi_0\frac{0.1x_2}{(R-r_w)\sqrt{x_1^2+x_2^2}}.$$

Rather than use the formulation in the second last column of Table 2, the full expressions in Cartesian coordinates as given in Table 2, column 3, were coded up and plotted in Fig. 6. The results are all axisymmetric with the forces pointing towards the center, giving confidence that the derivation and coding has been done correctly. Thus, the analytical results in the second last column were confirmed to give the same numerical results as column 3 for this problem.

Comparing Fig. 6 **(a)** and **(b)** shows that for this somewhat realistic analytical case, the term $\boldsymbol{M}\times(\nabla\times\boldsymbol{B})$ and the gradients in susceptibility (see Table 2 final column) do not contribute greatly to the calculated body force with only 2% greater maximum body force ($f_{b,max}$) for case (a) compared with case (b). The maximum body force in case (c) is nearly double that of case (b).

As expected from the second last column of Table 2, cases (d), (e) and (f) all give the same result, but it is less than half (41%) of the maximum body force calculated for case (b), our recommended formulation.

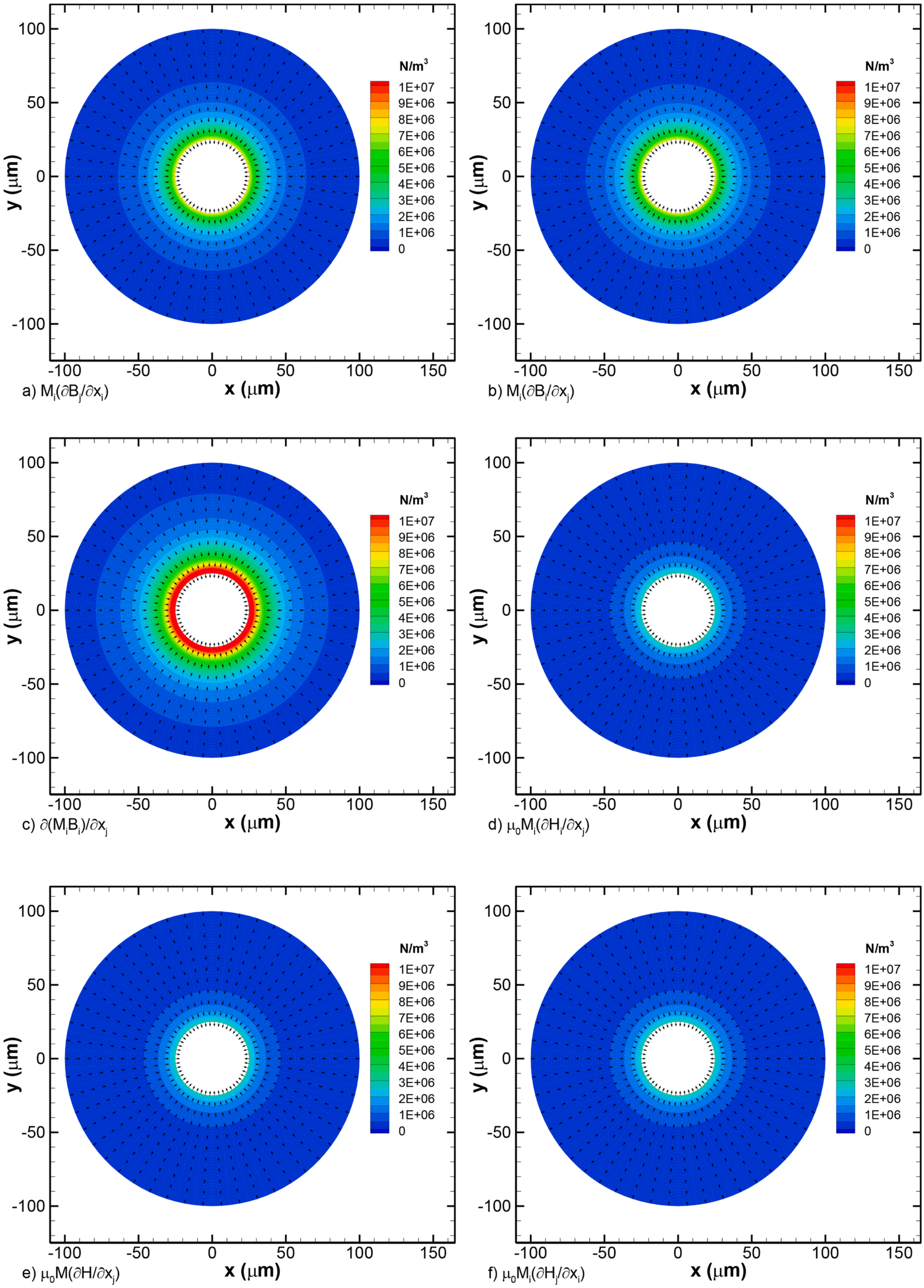

Fig. 6. Comparison of formulations for magnetic body force applied to ferrofluid surrounding a conducting wire. The cases (a) to (f) correspond to (a) to (f) in Table 2.

5.2. Effect on thermomagnetic convection

It can be anticipated from Fig. 6 that variation in body force will also affect thermomagnetic convection, which is a phenomenon driven by temperature gradients in magnetic fluids in the presence of a magnetic field. Temperature affects the body force because magnetization is a function of temperature due to Brownian motion randomly misaligning the magnetic particles. A number of temperature – magnetization relations have been proposed and are used in the literature. For example, in the Langevin approach (e.g. used by Kumar et al., 2021), the magnitude of the magnetization is a function of both temperature and magnetic field strength:

$$M(T,H) = M_\infty(coth(\alpha(T,H)) - 1\,/\,\alpha(T,H)), \tag{32}$$

where M and H are magnitudes of magnetization and magnetic field strength, M_∞ is the saturation magnetization of the fluid and: $\alpha(T,H) = \frac{\mu_0 M_s(T) V_p H}{k_B T}$. where M_s is the magnetization of the solid material, V_p is the volume of the particle, and k_B is the Boltzmann constant. In terms of the current formulation, the temperature dependence of magnetization enters the model via susceptibility, χ. Making use of the relationship $M = \chi H$, the susceptibility can be expressed as a function of temperature and magnitude of magnetic field strength:

$$\chi(T,H) = M_\infty(coth(\alpha(T,H)) - 1\,/\,\alpha(T,H))\Big/H \approx \frac{\mu_0 M_\infty M_s(T) V_p}{3k_B T}$$

where the approximation corresponds to the limit of small α (e.g. due to small H), so that the Langevin factor, $(coth(\alpha) - 1\,/\alpha) \approx \alpha\,/3$. This limit is referred to as the 'initial susceptibility' which is a function of temperature but not H.

To quantify the effect of the body-force formulation on thermomagnetic convection, different forms of body force terms derived in the last column of Table 2 (cases (a), (b), (c), and (d)), are applied in radial direction of ferrofluid, via compiling a user-defined function (UDF) in the computational fluid dynamics package, Ansys FLUENT 2021R2. A 2D axis-symmetric model is developed to measure the transient temperature of copper micro-wire and results are compared with experimental findings of Kumar et al. (2021).

The experimental results are from our previous published work where a 2A direct current was applied for 5s to a copper micro-wire of diameter 50 μm in a ferrofluid ($\phi = 2\%$ and $d_p = 10\ nm$). The current generates a self-induced magnetic field and Joule heating around the micro-wire. The value of initial susceptibility (χ_0) of tested ferrofluid is 1.88. Details on model development and governing equations are obtainable from Kumar et al. (2021). The model here is as described previously in Kumar et al. (2021) except that different body force formulations are being applied. Note that the magnetic force is only applied in the radial direction in the simulation and for simplicity, the simulation assumes the magnetic strength $\boldsymbol{H}$ is independent of the material properties and is that of

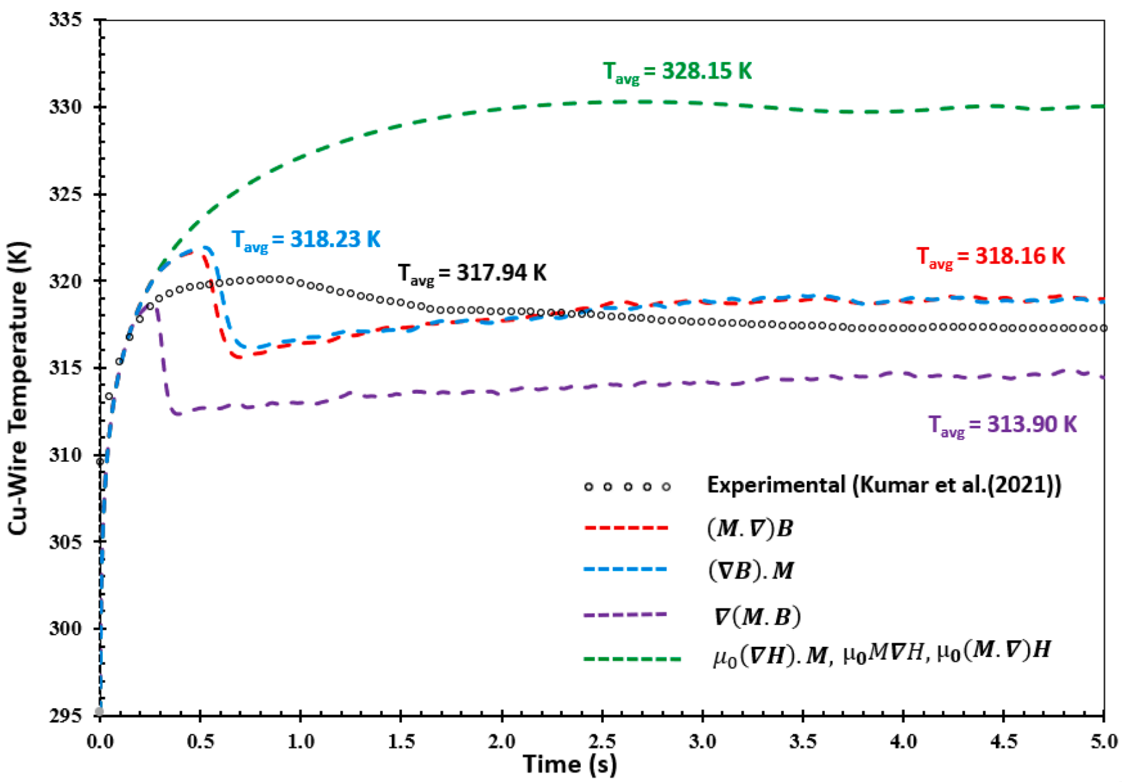

Fig. 7. Transient temperature of wire under difference body force terms

an infinitely long conductor. Gravitational buoyancy forces are applied axially.

Fig. 7 compares the experimental and simulation results for the heated wire temperature under the effect of thermomagnetic convection in the tested ferrofluid. These results suggest that all the body force models identify the phenomenon, but the results are significantly different. The wire temperature for proposed body force term $\boldsymbol{f}_b = (\nabla\boldsymbol{B})\cdot\boldsymbol{M}$ and term $\boldsymbol{f}_b = (\boldsymbol{M}\cdot\nabla)\boldsymbol{B}$ is close to correctly predicting the wire temperature and thermomagnetic cooling effect. In contrast, the term $\nabla(\boldsymbol{M}\cdot\boldsymbol{B})$ overpredicts the cooling effect and inception of thermomagnetic convection effects are earlier. In case of $\mu_0(\nabla\boldsymbol{H})\cdot\boldsymbol{M}$, the thermomagnetic convection effect is much less significant, resulting in less cooling and an overall higher temperature of wire. Overall, among the cases in Fig. 7 there is a variation of about 14 K, which is very significant, noting that the maximum temperature rise from the initial ambient temperature is about 28 K.

The oscillations in the simulation results shown in Fig. 7 are due to transient thermomagnetic convection effects near the wire. The calculated instantaneous temperature distributions shown in Fig. 8 show this effect for four different body-force configurations. We can see in Fig. 8**(c)**, due to the larger magnitude of $\boldsymbol{f}_b = \nabla(\boldsymbol{M}\cdot\boldsymbol{B})$ compared to the other cases, greater convection of heat from the wire into the fluid occurs with multiple rapid and irregular thermal eddies developing near wire surface. In Fig. 8**(a)** and **(b)** the number of eddies is reduced compared with Fig. 8**(c)**. This oscillating phenomenon is not so evident in the experimental results – possibly because of the three-dimensionality of the actual flow in contrast with the axisymmetric model. In the case of $\boldsymbol{f}_b = \mu_0(\boldsymbol{M}\cdot\nabla)\boldsymbol{H}$, natural convection dominates over thermomagnetic convection, which suppresses the cooling effect. Thus, Figs. 7 and 8 demonstrate that the form of the body force term has a very important influence on predicting thermomagnetic convection effects.

The differences between the experimental results and the predictions for the case of $\boldsymbol{f}_b = (\nabla\boldsymbol{B})\cdot\boldsymbol{M}$ in Fig. 7 may be attributed to model simplifications and an incomplete understanding of the importance of various secondary effects on thermomagnetic convection around a heated microwire. The model does not include magneto-viscous effects, magneto-phoresis effects or thermophoresis effects. The choice of the relation for modelling the temperature dependence of magnetic susceptibility is another consideration. Noting that other studies on thermomagnetic convection around larger conductors have reported convection cells in the r-θ plane (Krakov & Nikiforov, 2020), the axisymmetric assumption used in this simulation also may not be correct. Moreover, the infinite wire assumption for the magnetic field and the neglect of axial magnetic body forces in the simulation, removes finite-wire end effects on the magnetic field. These considerations should be explored in future studies.

6. Merits and originality of the present derivations

The main contributions of this study are the new derivations of the magnetic body force term from the Lorentz force and the magnetostatic forms of Maxwell's equations. Noting that Liu (2000) also proposed the same mathematical form for the body force (i.e. Eq. (14)), it is worthwhile highlighting the originality of our approach. Liu started with an expression representing the Helmholtz force (which itself appears to have been derived from a form of the Maxwell stress tensor according to Luo et al (2000)), and showed that the expression $\mu_0 M_i \nabla H_i$ can be derived if the susceptibility is a linear function of the density of magnetic particles (i.e. magnetic particle concentration, ρ). This assumption is expected to be correct in the limit of small χ (i.e. dilute ferrofluid), since higher order terms (ρ^2, ρ^3, …) in a general polynomial relation between χ and ρ will vanish if ρ is small. Liu further reasoned that if $\chi/(1+\chi)$ was taken as being proportional to ρ, it would be equally valid to arrive at $M_i \nabla B_i$ as the Kelvin body force from the Helmholtz force expression. This second assumption is more in line with our work since rather than χ, the components of magnetization (encircling bound current per unit length in each direction) should be proportional to ρ and from Eqs (4) and (7) $\boldsymbol{M} = (\chi/(1+\chi)\mu_0)\boldsymbol{B}$, indicating the importance of the ratio $\chi/(1+\chi)$. Thus, the derivations in this study complement Liu's work since we have started from the Maxwell equations and macroscopic definitions of all parameters to derive the magnetic force rather than making use of the abovementioned Helmholtz force expression.

A further feature of our study is the inclusion of definitions for all macroscopic magnetic parameters. This is not often done, but we believe it is useful because the literature contains subtly different definitions for the same parameters (e.g. Eq. (4) in this study is taken from Jackson (1999) as the macroscopic definition of $\boldsymbol{H}$ while Rosensweig (1987) uses the same equation as the definition of $\boldsymbol{M}$). Moreover, we are not aware of another study that interprets the components of the magnetization vector as encircling bound current per unit length in each direction. This understanding is useful because it is consistent with $\boldsymbol{M}$ being the magnetic moment density and makes it easy to write down the bound current term in Ampere's law (Eq. (8)).

7. Conclusions

To help clarify the significance of the different formulations for the magnetic body force term, we have presented a new derivation of the term and compared it with other formulations from the literature commonly used in last five years. Our derived term $(\nabla\boldsymbol{B})\cdot\boldsymbol{M}$ is the same as that recommended by Odenbach and Liu (2001) and Liu (2000) based on their theoretical and experimental work (their notation was $M_i \nabla B_i$). It differs by only a small amount from $(\boldsymbol{M}\cdot\nabla)\boldsymbol{B}$ based on a numerical example of a single conductor in ferrofluid. Equivalent formulations of the term are given by $(\boldsymbol{M}\times\nabla)\times\boldsymbol{B}$ and $(\boldsymbol{M}\cdot\nabla)\boldsymbol{B} + \boldsymbol{M}\times(\nabla\times\boldsymbol{B})$. Most of the formulations considered except $\nabla(\boldsymbol{M}\cdot\boldsymbol{B})$ approach the same result in the limit of small susceptibility ($\chi << 1$) which does not generally hold for ferrofluid. The proposed derivation requires that the differential volume experiencing the body force only contains complete dipole current loops. As a result, when using the term to model situations where the ferrofluid has interfaces with other materials (such as glass or air), an additional surface integral term to account for bound surface current is *not* needed since bound surface currents are already included in $(\nabla\boldsymbol{B})\cdot\boldsymbol{M}$. Some open questions still remain that could be resolved by rigorous experiments to better validate the proposed form of the term experimentally. The findings of this work are valuable for thermomagnetic convection and magnetophoresis studies and are not limited to ferrofluid but also apply to any other soft magnetic material for any value of χ.

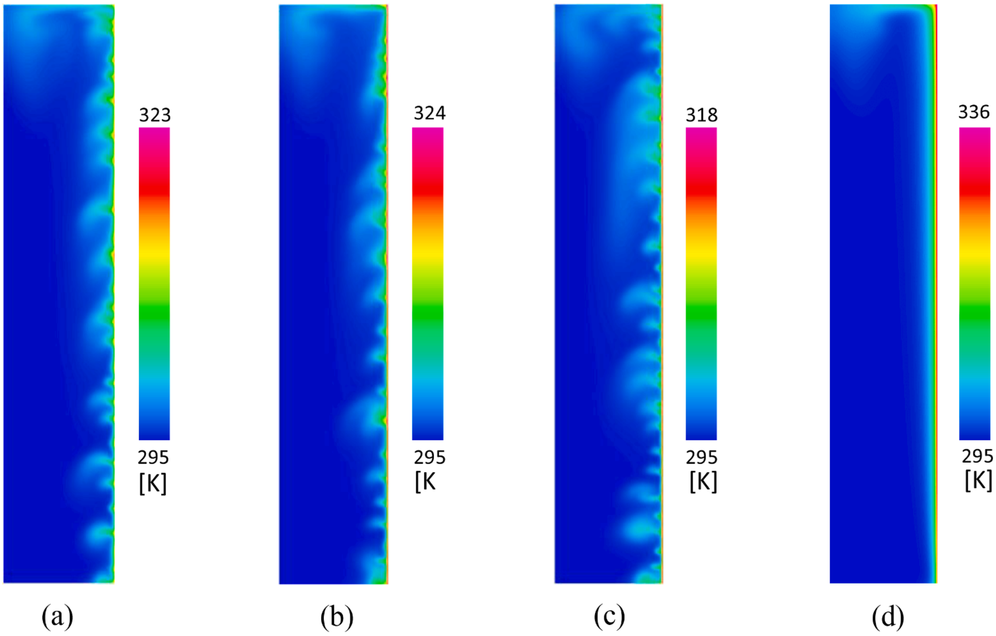

Fig. 8. Thermal field development at t =5s. The heated 50 μm diam., 43 mm long, vertical wire is on the right side of each of the images which show the full calculation domain (5 mm radius). (a) $(\boldsymbol{M}\cdot\nabla)\boldsymbol{B}$, (b) $(\nabla\boldsymbol{B})\cdot\boldsymbol{M}$, (c) $\nabla(\boldsymbol{M}\cdot\boldsymbol{B})$, (d) $\mu_0(\boldsymbol{M}\cdot\nabla)\boldsymbol{H}$.

Declaration of Competing Interest

The authors have no conflicts to disclose.

Data availability

Data will be made available on request.

Acknowledgements

The first author is thankful to Higher Degree Research scholarships from Griffith University.

Appendix –. Proof of Eq. (22) and Eq. (23)

An important step in the derivation from the integral forms of the Lorentz force is the proof of the following relationship:

$$\int_A (\boldsymbol{M}\times\widehat{\mathbf{n}})\times\boldsymbol{B}\,\mathrm{d}A = \int_V [(\nabla\boldsymbol{M})\cdot\boldsymbol{B} + (\nabla\boldsymbol{B})\cdot\boldsymbol{M} - (\nabla\cdot\boldsymbol{B})\boldsymbol{M} - \boldsymbol{B}\cdot(\nabla\boldsymbol{M})]\mathrm{d}V. \tag{A1}$$

Through a cross product vector identity, the LHS of **Eq. (A1)** can be rewritten as:

$$\int_A (\boldsymbol{M}\times\widehat{\mathbf{n}})\times\boldsymbol{B}\,\mathrm{d}A = \int_A [-\widehat{\mathbf{n}}\cdot(\boldsymbol{B}\otimes\boldsymbol{M}) + (\boldsymbol{M}\cdot\boldsymbol{B})\widehat{\boldsymbol{n}}]dA. \tag{A2}$$

Considering the first term in the integral on the RHS of Eq. (A2), this can be expanded as:

$$-\int_A \widehat{\boldsymbol{n}}\cdot(\boldsymbol{B}\otimes\boldsymbol{M})dA = -\int_A n_iB_iM_j\boldsymbol{e}_jdA. \tag{A3}$$

Applying the Gauss-Ostrogradsky theorem (Eremeyev et al. (2018)):

$$-\int_A n_iB_iM_j\boldsymbol{e}_jdA = -\int_V \left[\frac{\partial B_i}{\partial x_i}M_j + \frac{\partial M_j}{\partial x_i}B_i\right]\boldsymbol{e}_jdV = \int_V [-(\nabla\cdot\boldsymbol{B})\boldsymbol{M} - \boldsymbol{B}\cdot(\nabla\boldsymbol{M})]\mathrm{d}V. \tag{A4}$$

Similarly, considering the second term in the integral on the RHS of Eq. (A2):

$$\int_A (\boldsymbol{M}\cdot\boldsymbol{B})\widehat{\boldsymbol{n}}\,dA = \int_A M_i B_i n_j \boldsymbol{e}_j dA$$

$$= \int_V \left[\frac{\partial M_i}{\partial x_j}B_i + \frac{\partial B_i}{\partial x_j}M_i\right]\boldsymbol{e}_j dV$$

$$= \int_V [(\nabla\boldsymbol{M})\cdot\boldsymbol{B} + (\nabla\boldsymbol{B})\cdot\boldsymbol{M}]\mathrm{d}V. \tag{A5}$$

Substituting Eqs. (A4) and **(**A5**)** into Eq. (A2) gives **Eq. (A1).**

A further important relation in the derivation is needed to support Eq. (23):

$$(\nabla\times\boldsymbol{M})\times\boldsymbol{B} \;= -(\nabla\boldsymbol{M})\cdot\boldsymbol{B} + \boldsymbol{B}\cdot(\nabla\boldsymbol{M}). \tag{A6}$$

The proof can be made by rewriting LHS of Eq. (A6) in indicial form:

$$(\nabla\times\boldsymbol{M})\times\boldsymbol{B} \;= \left[\boldsymbol{e}_i\times\frac{\partial M_j}{\partial x_i}\boldsymbol{e}_j\right]\times B_k\boldsymbol{e}_k = \left[\frac{\partial M_j}{\partial x_i}\boldsymbol{e}_i\times\boldsymbol{e}_j\right]\times B_k\boldsymbol{e}_k$$

$$= \frac{\partial M_j}{\partial x_i}\varepsilon_{ijl}\boldsymbol{e}_l\times B_k\boldsymbol{e}_k = \frac{\partial M_j}{\partial x_i}B_k\varepsilon_{ijl}\varepsilon_{lkm}\boldsymbol{e}_m$$

$$= \frac{\partial M_j}{\partial x_i}B_k\boldsymbol{e}_m\left(-\delta_{jk}\delta_{im} + \delta_{jm}\delta_{ik}\right) = -\frac{\partial M_j}{\partial x_i}B_j\boldsymbol{e}_i + \frac{\partial M_j}{\partial x_i}B_i\boldsymbol{e}_j$$

$$= -\boldsymbol{e}_i\frac{\partial M_j}{\partial x_i}B_j + B_i\frac{\partial M_j}{\partial x_i}\boldsymbol{e}_j = -(\nabla\boldsymbol{M})\cdot\boldsymbol{B} + \boldsymbol{B}\cdot(\nabla\boldsymbol{M})$$

References

Aminfar, H., Mohammadpourfard, M., & Mohseni, F. (2012). Two-phase mixture model simulation of the hydro-thermal behavior of an electrical conductive ferrofluid in the presence of magnetic fields. *Journal of Magnetism and Magnetic Materials, 324*(5), 830–842.

Aminfar, H., Mohammadpourfard, M., & Zonouzi, S. A. (2013). Numerical study of the ferrofluid flow and heat transfer through a rectangular duct in the presence of a non-uniform transverse magnetic field. *Journal of Magnetism and Magnetic materials, 327*, 31–42.

Ashouri, M., & Shafii, M. B. (2017). Numerical simulation of magnetic convection ferrofluid flow in a permanent magnet–inserted cavity. *Journal of Magnetism and Magnetic Materials, 442*, 270–278.

Bahiraei, M., Hangi, M., & Rahbari, A. (2019). A two-phase simulation of convective heat transfer characteristics of water–Fe3O4 ferrofluid in a square channel under the effect of permanent magnet. *Applied Thermal Engineering, 147*, 991–997.

Bakuzis, A. F., Chen, K., Luo, W., & Zhuang, H. (2005). Magnetic body force. *Int. J. Mod. Phys. B, 19*, 205–1208.

Brand, L. (2020). *Vector and tensor analysis*. Courier Dover Publications.

Butcher, T. A., & Coey, J. M. D. (2023). Magnetic forces in paramagnetic fluids. *Journal of Physics: Condensed Matter, 35*(5), Article 053002.

Chapman, S. J. (2004). *Electric machinery fundamentals*. McGraw-Hill.

Cano-Gómez, G., & Romero-Calvo, Á. (2022). Comment on 'The magnetic body force in ferrofluids. *Journal of Physics D: Applied Physics, 55*(12), Article 128002.

Cecchini, L., & Chiolerio, A. (2021a). The magnetic body force in ferrofluids. *Journal of Physics D: Applied Physics, 54*(35), Article 355002.

Cecchini, L., & Chiolerio, A. (2021b). Reply to comment on 'The magnetic body force in ferrofluids. *Journal of Physics D: Applied Physics, 55*(12), Article 128001.

Dixit, D. D., & Pattamatta, A. (2020). Effect of uniform external magnetic-field on natural convection heat transfer in a cubical cavity filled with magnetic nano-dispersion. *International Journal of Heat and Mass Transfer, 146*, Article 118828.

Engel, A. (2001). Comment on "Invalidation of the Kelvin Force in Ferrofluids. *Physical Review Letters, 86*(21), 4978.

Eremeyev, V. A., Cloud, M. J., & Lebedev, L. P. (2018). *Applications of tensor analysis in continuum mechanics*.

Fadaei, F., Dehkordi, A. M., Shahrokhi, M., & Abbasi, Z. (2017). Convective-heat transfer of magnetic-sensitive nanofluids in the presence of rotating magnetic field. *Applied Thermal Engineering, 116*, 329–343.

Ganguly, R., Sen, S., & Puri, I. K. (2004). Heat transfer augmentation using a magnetic fluid under the influence of a line dipole. *Journal of Magnetism and Magnetic Materials, 271*(1), 63–73.

Ghosh, D., Meena, P. R., & Das, P. K. (2021). Heat transfer from a ferrofluid during generalized Couette flow through parallel plates in the presence of an orthogonal magnetic field. *International Journal of Thermal Sciences, 164*, Article 106895.

Goharkhah, M., Bezaatpour, M., & Javar, D. (2020). A comparative investigation on the accuracy of magnetic force models in ferrohydrodynamics. *Powder Technology, 360*, 1143–1156.

Hangi, M., Bahiraei, M., & Rahbari, A. (2018). Forced convection of a temperature-sensitive ferrofluid in presence of magnetic field of electrical current-carrying wire: A two-phase approach. *Advanced Powder Technology, 29*(9), 2168–2175.

Huang, L., Hädrich, T., & Michels, D. L. (2019). On the accurate large-scale simulation of ferrofluids. *ACM Transactions on Graphics (TOG), 38*(4), 1–15.

Jackson, J. D. (1999). *Classical Electrodynamics* (3rd Edition). USA: Wiley.

Khashan, S. A., Elnajjar, E., & Haik, Y. (2011a). Numerical simulation of the continuous biomagnetic separation in a two-dimensional channel. *International journal of multiphase flow, 37*(8), 947–955.

Khashan, S. A., Elnajjar, E., & Haik, Y. (2011b). CFD simulation of the magnetophoretic separation in a microchannel. *Journal of Magnetism and Magnetic Materials, 323*(23), 2960–2967.

Krakov, M. S., & Nikiforov, I. V. (2020). Influence of the shape of the inner boundary on thermomagnetic convection in the annulus between horizontal cylinders: Heat transfer enhancement. *International Journal of Thermal Sciences, 153*, Article 106374.

Kuo, K. K. Y., & Acharya, R. (2012). *Applications of turbulent and multiphase combustion*. John Wiley & Sons.
Kumar, V., Casel, M., Dau, V., & Woodfield, P. (2021). Effect of axisymmetric magnetic field strength on heat transfer from a current-carrying micro-wire in ferrofluid. *International Journal of Thermal Sciences, 167*, Article 106976.
Leong, S. S., Ahmad, Z., & Lim, J. (2015). Magnetophoresis of superparamagnetic nanoparticles at low field gradient: hydrodynamic effect. *Soft Matter, 11*(35), 6968–6980.
Liu, M. (2000). Range of validity for the Kelvin force. *Physical Review Letters, 84*(12), 2762.
Luo, W., Du, T., & Huang, J. (2000). Luo, du, and huang reply. *Physical Review Letters, 84*(12), 2763.
Mukhopadhyay, A., Ganguly, R., Sen, S., & Puri, I. K. (2005). A scaling analysis to characterize thermomagnetic convection. *International Journal of Heat and Mass Transfer, 48*(17), 3485–3492.
Neuringer, J. L., & Rosensweig, R. E. (1964). *Ferrohydrodynamics. The Physics of Fluids, 7*(12), 1927–1937.
Nguyen, N. T. (2012). Micro-magnetofluidics: interactions between magnetism and fluid flow on the microscale. *Microfluidics and nanofluidics, 12*(1), 1–16.
Odenbach, S., & Liu, M. (2001). Invalidation of the Kelvin force in ferrofluids. *Physical review letters, 86*(2), 328.
Papanastasiou, T., Georgiou, G., & Alexandrou, A. N. (2021). *Viscous fluid flow*. CRC press.
Petit, M., Kedous-Lebouc, A., Avenas, Y., Tawk, M., & Artega, E. (2011). Calculation and analysis of local magnetic forces in ferrofluids. przeglad elektrotechniczny. *(Electrical Review), 87*(9b), 115–119.
Priyadharsini, S., & Sivaraj, C. (2022). Numerical simulation of thermo-magnetic convection and entropy production in a ferrofluid filled square chamber with effects of heat generating solid body. *International Communications in Heat and Mass Transfer, 131*, Article 105753.
Rahman, H., & Suslov, S. A. (2015). Thermomagnetic convection in a layer of ferrofluid placed in a uniform oblique external magnetic field. *Journal of Fluid Mechanics, 764*, 316–348.
Romero-Calvo, Á., Cano-Gómez, G., Hermans, T. H., Benítez, L. P., Gutiérrez, M. A. H., & Castro-Hernández, E. (2020). Total magnetic force on a ferrofluid droplet in microgravity. *Experimental Thermal and Fluid Science, 117*, Article 110124.
Rong, Z., Iwamoto, Y., & Ido, Y. (2022). Thermal flow analysis of self-driven temperature sensitive magnetic fluid between partially heated parallel plates. *Journal of Magnetism and Magnetic Materials, 552*, Article 169079.
Rosensweig, R. E. (1987). *Magnetic fluids. Annual review of fluid mechanics, 19*(1), 437–461.
Saedi, M., Aminfar, H., Mohammadpourfard, M., & Maroofiazar, R. (2019). Simulation of ferrofluid flow boiling in helical tubes using two-fluid model. Heat and Mass Transfer, 55(1), 133-148.
Shaker, H., Abbasalizadeh, M., Khalilarya, S., & Motlagh, S. Y. (2021). Two-phase modeling of the effect of non-uniform magnetic field on mixed convection of magnetic nanofluid inside an open cavity. *International Journal of Mechanical Sciences, 207*, Article 106666.
Shakiba, A., & Vahedi, K. (2016). Numerical analysis of magnetic field effects on hydro-thermal behavior of a magnetic nanofluid in a double pipe heat exchanger. *Journal of Magnetism and Magnetic Materials, 402*, 131–142.
Soltanipour, H. (2020). Two-phase simulation of magnetic field effect on the ferrofluid forced convection in a pipe considering Brownian diffusion, thermophoresis, and magnetophoresis. *The European Physical Journal Plus, 135*(9), 1–23.
Sun, J., Shi, Z., Chen, S., & Jia, S. (2019). Experimental and numerical analysis of the magnetophoresis of magnetic nanoparticles under the influence of cylindrical permanent magnet. *Journal of Magnetism and Magnetic Materials, 475*, 703–714.
Vatani, A., Woodfield, P. L., Nguyen, N. T., Abdollahi, A., & Dao, D. V. (2019). Numerical simulation of combined natural and thermomagnetic convection around a current carrying wire in ferrofluid. *Journal of Magnetism and Magnetic Materials, 489*, Article 165383.
Vatani, A., Woodfield, P. L., Nguyen, N. T., & Dao, D. V. (2017). Thermomagnetic convection around a current-carrying wire in ferrofluid. *Journal of Heat Transfer*, (10), 139.